THE ASTROPHYSICAL JOURNAL, 542:251–256, 2000 October 10

RAPID OPTICAL FOLLOW-UP OBSERVATIONS OF SGR EVENTS WITH ROTSE-I

C. AKERLOF,[1] R. BALSANO,[2] S. BARTHELMY,[3] J. BLOCH,[2] P. BUTTERWORTH,[3] D. CASPERSON,[2] T. CLINE,[3] S. FLETCHER,[2] G. GISLER,[2] J. HILLS,[2] R. KEHOE,[1] B. LEE,[1,4] S. MARSHALL,[5] T. MCKAY,[1] A. PAWL,[1] W. PRIEDHORSKY,[2] N. SELDOMRIDGE,[2] J. SZYMANSKI,[2] AND J. WREN[2]

Received 2000 March 27; accepted 2000 May 18

ABSTRACT

In order to observe nearly simultaneous emission from gamma-ray bursts (GRBs), the Robotic Optical Transient Search Experiment (ROTSE) receives triggers via the GRB Coordinates Network (GCN). Since beginning operations in 1998 March, ROTSE has also taken useful data for 10 SGR events: eight from SGR 1900+14 and two from SGR 1806−20. We have searched for new or variable sources in the error regions of these SGRs, and no optical counterparts were observed. Limits are in the range $m_{\rm ROTSE} \approx 12.5$–15.5 during the period 20 s to 1 hr after the observed SGR events.

Subject headings: gamma rays: bursts — gamma rays: observations — pulsars: individual (SGR 1900+14, SGR 1806−20)

1. INTRODUCTION

Soft gamma-ray repeaters (SGRs) were separated from classical gamma-ray bursts (GRBs) based on the repetition of transient events from a single source and their soft spectra (Mazets & Golenskii 1981; Atteia et al. 1987; Laros et al. 1987), which are generally well fitted by an optically thin thermal bremsstrahlung model (Norris et al. 1991). The events tend to be short ($\sim$0.1 s) but on occasion have been observed for hundreds of seconds (e.g., the 1979 March 5 [Mazets et al. 1979] and 1998 August 27 giant flares [Cline, Mazets, & Golenetskii 1998; Hurley et al. 1999c; Mazets et al. 1999]). The positions of SGRs are all near or in supernova remnants (Cline et al. 1982; Kulkarni & Frail 1993; Vasisht et al. 1994; Hurley et al. 1999a; Woods et al. 1998), and all have quiescent X-ray counterparts (Murakami et al. 1994; Hurley et al. 1999b; Rothschild, Kulkarni, & Lingenfelter 1994; Woods et al. 1999). The quiescent X-ray counterparts to SGR 1900+14 (Hurley et al. 1999b), SGR 1806−20 (Kouveliotou et al. 1998), and possibly SGR 1627−41 (Woods et al. 1999); but see also Hurley et al. 2000) are X-ray pulsars with several second periods. Furthermore, these pulsars show spin-down periods which imply dipole magnetic fields of $\approx 10^{14}$–10^{15} G (Kouveliotou et al. 1998, 1999). This evidence strongly suggests that the sources of SGR events are highly magnetized, young neutron stars (magnetars) (Duncan & Thompson 1992) in which magnetically induced "starquakes" result in the sudden release of γ-rays (Thompson & Duncan 1995).

There is currently nothing known about the spectrum of SGR bursts at energies below a few keV. In this paper we present optical observations of SGR locations contemporaneous with SGR γ-ray events. The Robotic Optical Transient Search Experiment (ROTSE) (Kehoe et al. 1999) is configured to respond to transient events from the Gamma-Ray Burst Coordinates Network (GCN) (Barthelmy et al. 1995) and is capable of rapidly slewing to the coordinates of a transient event such as an SGR burst.[6] Since beginning operations in 1998 March, the first-generation system, ROTSE-I, has triggered on 16 SGR events. For all of these events, GCN alerts were based on data from the Burst and Transient Source Experiment (BATSE) (Fishman et al. 1989).

2. OBSERVATIONS

A typical ROTSE-I response to a BATSE-derived GCN trigger consists of a series of direct exposures centered at the trigger coordinates followed by a series of tiled exposures with the mount shifted by $\pm 8^\circ$ (half the total field of view) in both right ascension and declination to extend ROTSE-I's coverage of the GCN error box. The duration of the exposures and the number of times the direct/tile sequence is repeated depend on the type of trigger received from GCN and its typical delay from the onset of the trigger event. Currently, ROTSE-I makes no distinction in its response to GRBs and SGRs. Most GCN triggers arrive $\sim$5 s after the start of a burst, while some are delayed 5–11 minutes. ROTSE-I generally begins observations less than 5 s after receiving a GCN trigger. For observations begun within a few minutes of a burst, image exposure lengths start at 5 s and are extended first to 25 s and then to 125 s. In 1999 we reduced the latter two exposure lengths to 20 s and 80 s, respectively.

ROTSE-I has responded to 16 SGR triggers. Of these, useful data were obtained for eight SGR 1900+14 bursts and for two SGR 1806−20 bursts. Sample corrected images for both sources are shown in Figure 1. For most of these events, the first useful images are delayed by over 2 minutes, either because the SGR position is only in tiled images or because a disproportionate number of SGR triggers were of the delayed types.[7] The exception is BATSE trigger 6809, for which we have images starting less than 20 s after the burst and continuing for 1 hr. The durations of the SGR bursts were all less than 1 s with the exception of BATSE trigger 6798, which was a series of bursts emitted over a period of 350 s. In the response to this trigger, two ROTSE images follow emission spikes by less than 5 s

[1] University of Michigan, Ann Arbor, MI 48109.
[2] Los Alamos National Laboratory, Los Alamos, NM 87545.
[3] NASA Goddard Space Flight Center, Greenbelt, MD 20771.
[4] Fermi National Accelerator Laboratory, Batavia, IL 60510.
[5] Lawrence Livermore National Laboratory, Livermore, CA 94550.
[6] GCN Web page available at http://gcn.gsfc.nasa.gov/gcn.

[7] The known SGR position errors are small compared to the ROTSE-I field of view, but the rapidly determined positions for short, soft-spectrum events are often subject to very large uncertainties.

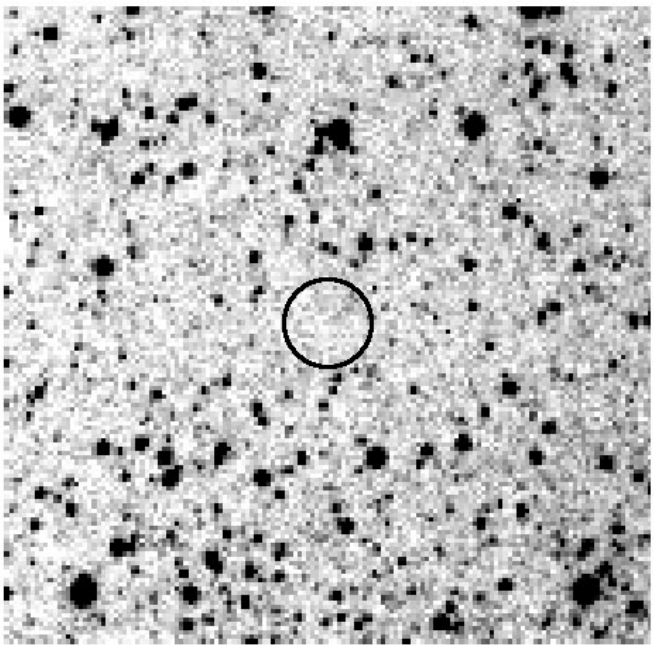

FIG. 1*a*

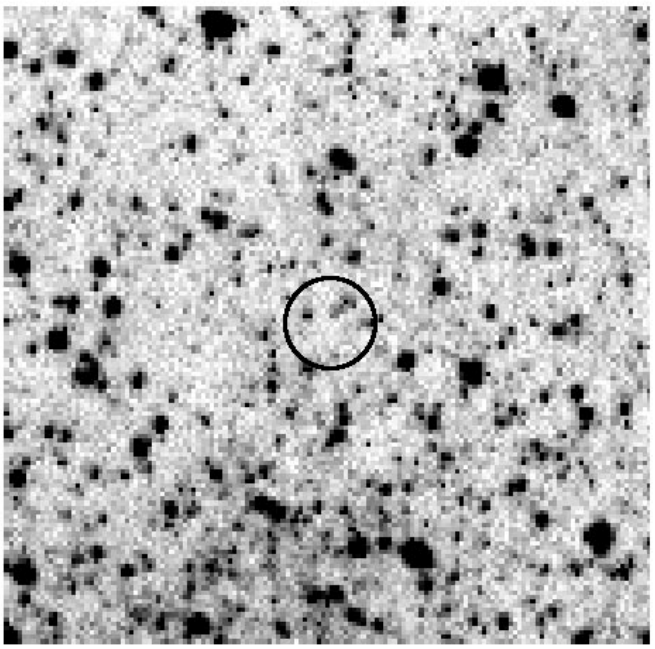

FIG. 1*b*

FIG. 1.—Sample ROTSE images for (*a*) SGR 1900+14 and (*b*) SGR 1806−20. Each image is ≈50′ wide. The adopted search region, which is 5′ in diameter, is circled.

(see Fig. 2). ROTSE-I SGR responses are summarized in Table 1.

2.1. *Data Reduction*

All images have been dark corrected and flat-fielded. All objects in an image are detected using SExtractor (Bertin & Arnouts 1996). The object lists are photometrically and astrometrically calibrated against the Tycho Reference Catalogue (Høg et al. 1998). Since ROTSE-I uses an unfiltered CCD, the photometry is color corrected using Tycho $B-V$ to produce a ROTSE-I equivalent V-band magnitude, $m_{\rm ROTSE}$. This procedure produces photometric errors as small as 0.02 mag for stars with $m_{\rm ROTSE} < 12$. The astrometric errors are typically 1.″4 (0.1 pixel).

2.2. *Discussion*

2.2.1. *Locations*

Currently available localizations for SGRs are a small fraction of the 16° × 16° ROTSE-I field of view, so only a small portion of any image must be searched for new or

TABLE 1

SUMMARY OF ROTSE-I SGR OBSERVATIONS

Date	Trigger	Peak Flux[a] (10^{-6} ergs cm^{-2} s^{-1})	Fluence[a] (10^{-7} ergs cm^{-2})	Δt (s)	$N_{\rm im}$	Comments[b]
			SGR 1900+14[c]			
980530.....	6798	20.4(2)	354(2)	168	4	Tiles
980607.....	6809	14.5(2)	29.3(2)	19	13	Direct
				1023	4	Tiles
980719.....	6932	2.35(5)	1.52(3)	226	1	Tiles, delayed trigger
				669	4	Tiles
980720.....	6934	0.71(3)	0.45(2)	316	23	Direct, delayed trigger
980921.....	7107	0.32(3)	0.24(3)	682	22	Direct, delayed trigger
980927.....	7124	5.32(7)	8.96(8)	153	4	Tiles, delayed trigger
				617	16[d]	Direct, delayed trigger
990429.....	7536	0.69(3)	0.54(2)	933	2	Tiles
990429.....	7537	0.93(4)	1.49(5)	831	4	Tiles
			SGR 1806−20			
980908.....	7073	1.44(4)	1.18(3)	425	6	Direct, first images cloudy
980922.....	7109	1.31(4)	0.98(2)	174	4	Tiles

NOTE.—Columns specify event date (yymmdd), BATSE trigger number, BATSE peak flux ($E > 25$ keV,64 ms timescale), BATSE fluence ($E > 25$ keV), delay before first usable image, number of usable images, and comments on the ROTSE data.

[a] P. Woods & E. Gögüs 2000, private communication.

[b] "Direct" means the SGR was in direct exposures, "tiles" that it was only in tiles.

[c] For three triggers, a second GCN trigger was received at a new location.

[d] This does not include six frames in which only half of the SGR error region was covered.

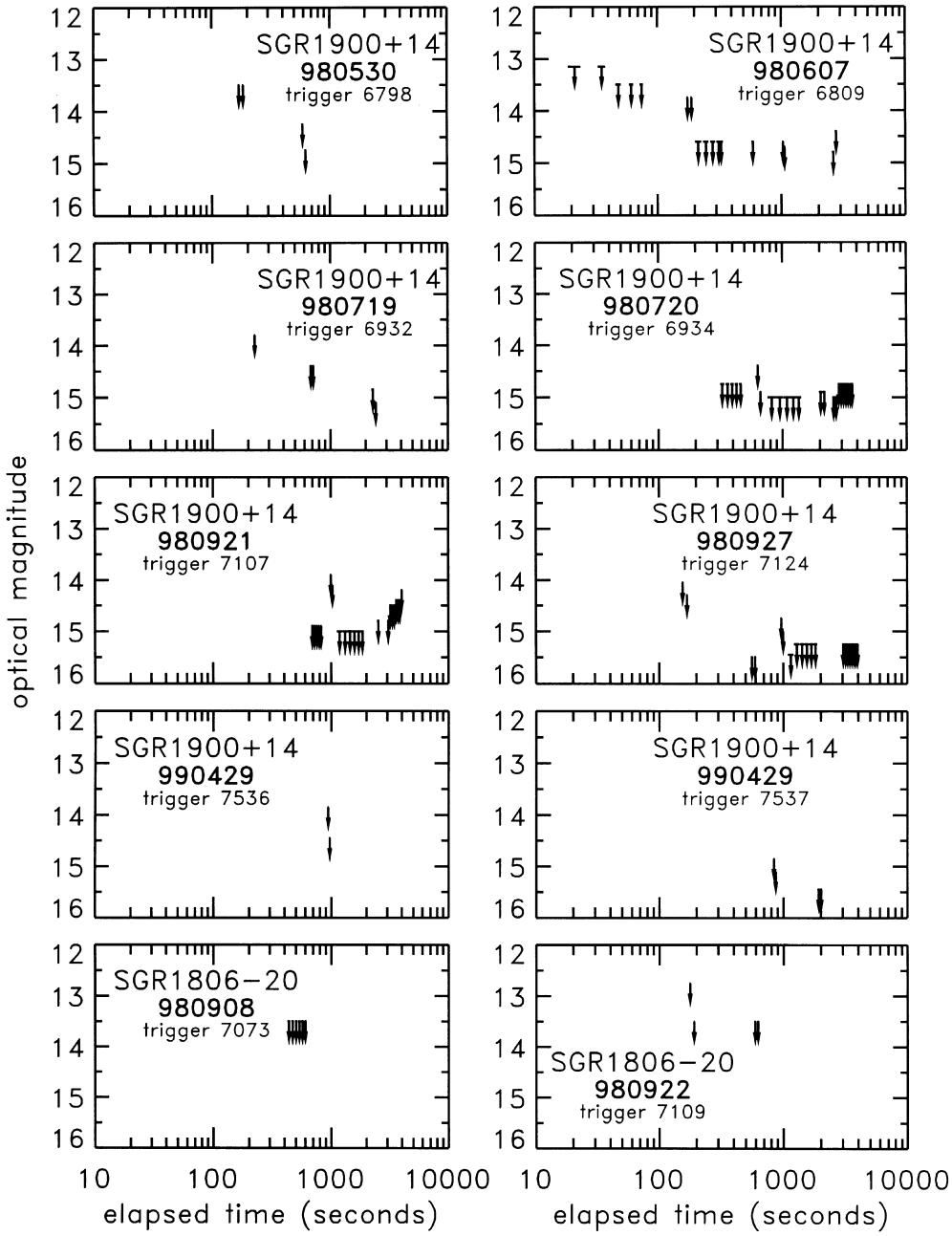

FIG. 2.—ROTSE magnitude limits, $m_{\rm ROTSE}$, for the 10 triggers with useful data. Each plot gives the limits, $m_{\rm ROTSE}$, as a function of delay since the SGR event start.

variable objects. The adopted search regions for SGR 1900+14 and SGR 1806−20 are centered on $\alpha(2000) = 19^{\rm h}7^{\rm m}14^{\rm s}$, $\delta(2000) = 9°20'$ and $\alpha(2000) = 18^{\rm h}8^{\rm m}39^{\rm s}$, $\delta(2000) = -20°24'40''$, respectively. In both cases we use a 2.″5 (10 pixel) radius search region. For SGR 1900+14 the search region is ≈100 times larger than the statistical IPN error region (Hurley et al. 1999d) and 10^6 times larger than the VLA error region (Frail et al. 1999). For SGR 1806−20 the search region is ≈300 times larger than the IPN error ellipse (Hurley et al. 1999d). The error regions are enlarged so that artificially added objects used to determine our efficiency (see below) do not always fall on the same pixels.

2.2.2. *Limits*

No new or variable objects were detected in any images within the specified search regions. Limits, shown in Figure 3, were obtained by determining at what magnitude our efficiency for detecting artificially added objects falls to 50%. For SGR 1806−20, we found these added objects with SExtractor. For SGR 1900+14, we searched by eye for the added objects in all images and used SExtractor for a subset of the images; a comparison between the methods indicates that agreement is within 0.25 mag. The limits are calculated in this manner to avoid two potential problems. First, the ROTSE-I plate scale is 14.″4 pixel^{-1} so that distinct catalog sources may blend into a single object in a ROTSE-I image. Second, $m_{\rm ROTSE}$ only corresponds to m_V on average, limiting the usefulness of single-object catalog comparisons.

2.2.3. *Extinction*

Since both SGR 1900+14 and SGR 1806−20 are at low Galactic latitudes, extinction is a large concern. Unfor-

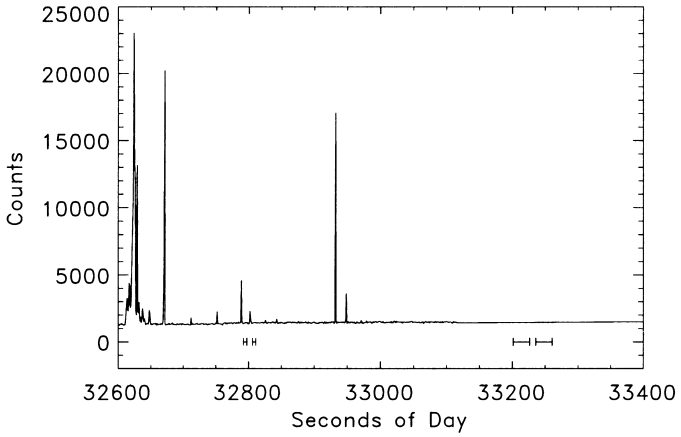

FIG. 3.—Raw counts for the SGR 1900+14 event 980530 (BATSE trigger 6798). The horizontal bars show the times of the ROTSE exposures for this event.

tunately, no direct measurements of the extinction to either SGR exist. However, infrared observations covering the IPN localization for SGR 1900+14 provide estimates of $A_V = 15.4 \pm 1.2$ mag at 2.2–6.6 kpc and $A_V = 19.1 \pm 1.2$ mag at 12–15 kpc (Vrba et al. 1996). To get an alternate estimate for the extinction to these SGRs, we turn to the X-ray data.

Both SGR 1900+14 and SGR 1806−20 have been detected as X-ray pulsars so that the hydrogen column density measured from the X-ray spectra can be used to estimate optical extinction via the relation $A_V = (4.5 \pm 0.3) \times 10^{-22} n_h$ mag (Gorenstein 1975). The stated error is entirely statistical while the dominant errors are likely to be systematic. Furthermore, this relation ignores the possible lack of correlation between X-ray absorption and optical extinction near the SGR itself. For example, if self-absorption of X-rays at the source is important, this relation will overestimate the optical extinction (see Gorenstein 1975 for a detailed discussion). Conversely, dust local to the SGR would necessitate increasing the optical extinction calculated by scaling to n_h. Nevertheless, this relation will provide us with useful estimates of the optical extinction.

SGR 1900+14 was detected as a pulsar by *ASCA*, and spectral fits gave a hydrogen column density of $n_h = (2.16 \pm 0.07) \times 10^{22}$ cm^{-2} and an estimated distance to the SGR of ~5 kpc (Hurley et al. 1999b), which agrees with the distance estimate to the supernova remnant G42.8+0.6 with which the SGR appears to be associated (Vasisht et al. 1994). Thus we obtain $A_V \approx 10$ mag and the equivalent extinctions in R and I bands of $A_R \approx 7$ mag and $A_I \approx 5$ mag (see, e.g., Cardelli et al. 1989), respectively.

For SGR 1806−20, $n_h \approx 6 \times 10^{22}$ cm^{-2} (Murakami et al. 1994; Sonobe et al. 1994) gives $A_V \approx 27$, $A_R \approx 20$, and $A_I \approx 13$. Given the enormous extinction to SGR 1806−20, we will restrict the remainder of the discussion to SGR 1900+14.

As discussed in § 2.1, the ROTSE-I system does not use a standard passband, so an estimate of the system's spectral response was required to understand the appropriate extinction value to adopt. In Figure 4*a*, the quantum efficiency of the Thomson CCD is shown along with measurements of the transmission of the Canon telephoto lens. The lens transmission above 0.65 μm was measured using a Ti-sapphire laser, and errors were estimated at a few percent. The lens transmission below 0.65 μm was measured with HeNe and GreNe lasers with errors less than 1%. The dashed curve in the figure is a linear least-squares fit to the Ti-sapphire data matched to a line through the HeNe and GreNe points. This simple parameterization is sufficient to investigate the effects of extinction on the spectral response

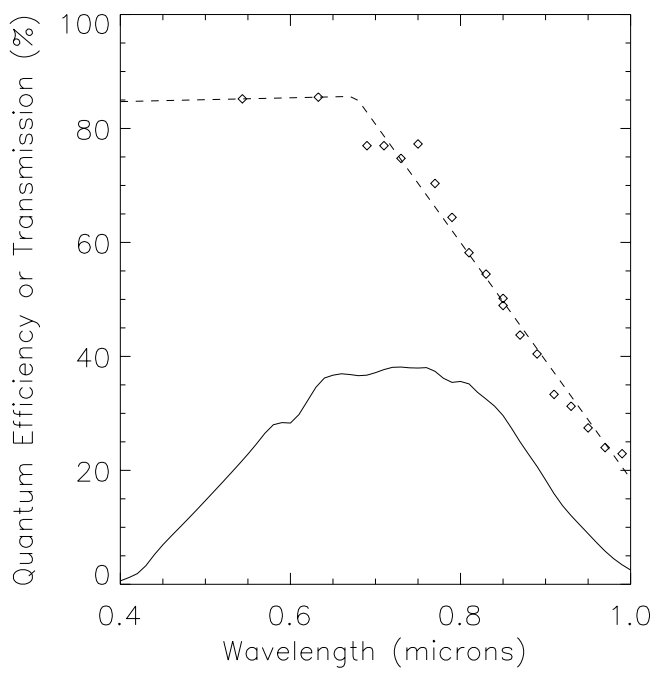

FIG. 4*a*

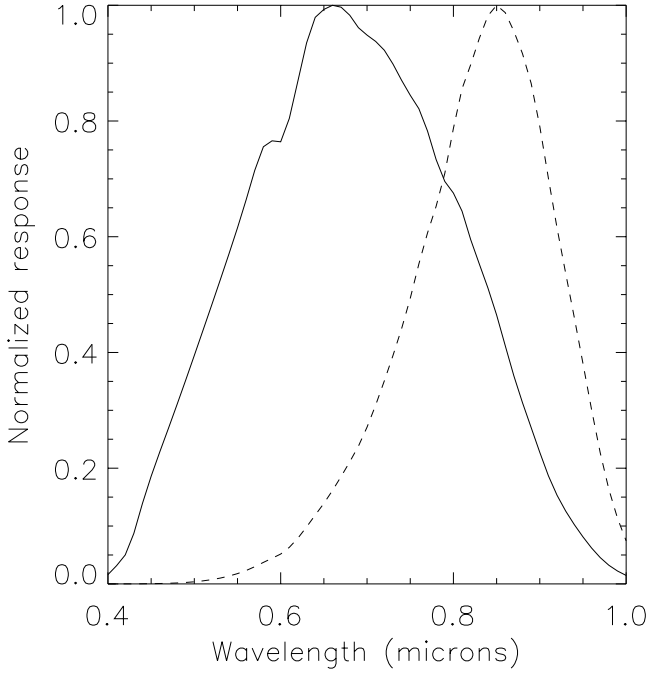

FIG. 4*b*

FIG. 4.—(*a*) A typical Thomson THX7899M CCD quantum efficiency (*solid line*) adapted from Thomson-CSF Semiconductors Specifiques (1995 December) and the transmission of the Canon FD 200 mm F1.8L lens (see text for a description of the measurements). (*b*) The normalized CCD+lens response (*solid line*) and the normalized effective response including an extinction curve with $A_V = 10$ from Cardelli et al. (1989) (*dashed line*).

of the system. In the right panel of Figure 4, the CCD quantum efficiency multiplied by the model of the lens transmission is shown along with this same curve additionally multiplied by an extinction curve with $A_V = 10$. There are three points to be noted about the ROTSE-I spectral response. First, although we quote an equivalent V-band magnitude, $m_{\rm ROTSE}$, the ROTSE-I system is best color matched to R band. Second, in the absence of extinction, the response is dominated by the CCD quantum efficiency which extends to ~ 1 μm. Finally, when the extinction is included, the spectral response is more closely matched to a narrow I-band filter. Given these complications, we will conservatively adopt $A_R \approx 7$ mag applied directly to our values of $m_{\rm ROTSE}$ for the remainder of this paper.

2.2.4. *Physical Interpretation of the Limits*

With the calculated extinction to SGR 1900+14, we can now address how bright an optical transient would have to be for ROTSE-I to detect it. Accepting the distance of ~ 5 kpc for SGR 1900+14, a typical ROTSE-I limit of $m_{\rm ROTSE} \approx 14$ mag gives an absolute magnitude limit of $M_{\rm ROTSE} \approx -1$. The extinction of $A_R \approx 7$ mag increases this limit to $M_V \approx -8$, about the brightness of a nova.

In the absence of firm predictions for the expected optical emission from SGRs following soft γ-ray events, we can only investigate constraints on possible sites for emission. There are two constraints with which we will be concerned: the ROTSE-1 magnitude limits expressed as a luminosity and the brightness temperature limits they imply assuming various emission regions. We will consider three possible sites for optical emission: the magnetar surface, a region comparable in size to the light cylinder (i.e., the radius at which field lines corotating with the neutron star would travel at the speed of light), and a nebula.

For what follows, we compute the luminosity limit implied by $m_{\rm ROTSE} > 14$. The spectral energy density, scaled to an extinction of $A_R = 7$ mag, is $f_\nu \leq 6 \times 10^{-23} \times 2.5^{7-A_R}$ ergs cm^{-2} s^{-1} Hz^{-1}. This corresponds to a limit on the isotropic optical luminosity of

$$L_{\rm opt} \leq 3 \times 10^{37} \times 2.5^{7-A_R} \text{ ergs s}^{-1} \sim 0.1 L_{\rm Edd} . \quad (1)$$

First, we investigate emission from near the magnetar surface. SGR events with rise and decay times unresolved with 5 ms time bins imply a source for the γ-rays less than 1500 km in extent (Kouveliotou et al. 1987). It is reasonable to assume that this emission arises near the magnetar surface.[8] SGR events are super-Eddington in the X-ray [$L \sim (10\text{–}10^3) \times L_{\rm Edd}$], so there is certainly sufficient energy released in the system to produce a luminosity $L_{\rm opt}$ comparable to that in equation (1). However, computing the brightness temperature via $T_b = f_\nu c^2 / 2\nu^2 k \Omega_s$ with Ω_s, the solid angle subtended by the source, gives

$$T_b < 5 \times 10^9 \text{ keV } d_5^2 \, r_{s,10}^{-2} , \quad (2)$$

where d_5 is the distance to the SGR is units of 5 kpc and $r_{s,10}$ is its radius in units of 10 km.[9] This should be compared with a typical temperature of $T \sim 25$ keV obtained in spectral fits to burst data or $T \sim 1$ keV for the neutron star surface. Therefore, the ROTSE-I limits do not constrain the optical emission from near the magnetar surface.

Next we consider optical emission from a region comparable in size to the magnetar's light cylinder, $r_{\rm lc} = 2.5 \times 10^5$ km. Here the ROTSE-1 limits imply $T_b < 8$ keV. At this distance, the magnetar's dipolar field strength, $B \sim 10^6$ G, gives an upper limit of $L \sim B^2 c R^2 \approx 10^{43}$ ergs s^{-1} to any radiation derived from magnetic field energy. The optical limits presented here are considerably lower than this, but we lack a plausible mechanism for producing optical emission at this distance scale.

Finally, we consider emission from a nebula energized by the SGR activity. Seven days after the giant flare of 1998 August 27, Frail et al. (1999) derive a lower limit on the size of the radio nebula around SGR 1900+14 of 100 μas. This can only be used as a rough estimate of the size relevant to the ROTSE-1 observations since it is a lower limit and it is derived at late times for a nebula which is presumed to be expanding. The implied limit on optical brightness temperature at the scale of $r_{\rm neb}$ is $T_b < 3 \times 10^{-3}$ keV.[10] This is well below the limit of $T_b = 3 \times 10^4$ keV for incoherent synchrotron emission. The only issue then is whether or not detectable luminosity could be generated in a nebula surrounding the SGR.

To estimate nebular optical luminosity, we closely follow Tavani (1994), using his scalings except where noted. During a super-Eddington SGR burst, a relativistic fireball is expected which will sweep up material in the medium surrounding the SGR, producing a shock which will dissipate energy via synchrotron radiation. Scaling to a γ-ray energy of $\sim 10^{40}$ ergs, the total energy of the burst is $E_{b,T} = 10^{40} \epsilon_r^{-1} E_{b,40}$ ergs, where ϵ_r is the efficiency of conversion of total burst energy into soft γ-rays and $E_{b,40}$ is the soft γ-ray energy scaled to 10^{40} ergs. The electron-positron pairs in the fireball will be energized by the shock and will radiate with a half-power lifetime of $\tau_s \sim 5 \times 10^8 \gamma_b^{-1} B^{-2} \sim 5 \times 10^2 \gamma_{b,6}^{-1} B^{-2}$, where B is the magnetic field and γ_b the Lorentz factor of $e^\pm$ pairs accelerated in the shock. We use $B \sim 1$ G as estimated from the VLA angular size lower limit (Frail et al. 1999) and $\gamma_b \sim 10^6$ as in Tavani (1994). To obtain the conversion efficiency, ϵ_s, from total burst energy to high-energy nebular emission, Tavani (1994) scales using the high-energy efficiency of the Crab Nebula, $\epsilon_s \sim$ 10%–20%, whereas for optical emission $\epsilon_s = 10^{-2} \epsilon_{s,-2}$ is a more appropriate estimate (see e.g., Manchester & Taylor 1977). We note that this is still likely to be an overestimate of the optical efficiency since the electron density of the optical emitting regions in the Crab Nebula is 10^3 cm^{-3} (see e.g., Manchester & Taylor 1977) while SGR 1900+14 is found outside SNR G42.8+0.6 (Vasisht et al. 1994), where one might expect densities 0.1–1 cm^{-3} (Taylor & Cordes 1993).

With the preceding relations, we can parameterize the expected optical luminosity from nebular emission as

$$L \simeq \frac{\epsilon_s E_{b,T}}{\tau_s} \sim (10^{35} \text{ ergs s}^{-1}) \epsilon_{s,-2} \epsilon_r^{-1} \gamma_6^{-1} B^{-2} E_{b,40} . \quad (3)$$

The luminosity limit in equation (1) is roughly 2 orders of magnitude greater than that estimated for nebular emission

[8] The size of a trapped, optically thick pair-photon plasma responsible for the emission might be at most $\sim$10–1000 times larger in area than the neutron star (R. Duncan 2000, private communication), which does not change the conclusion reached here.

[9] For a neutron star, $T \sim 1$ keV justifies the Rayleigh-Jeans form for blackbody emission.

[10] No longer making the Rayleigh-Jeans approximation.

in equation (3) and is therefore not particularly constraining. However, this type of emission is the most likely target for future observations of the type discussed in this paper.

2.2.5. *Comparison to Previous Work*

Pedersen et al. (1984) used a high-speed photoelectric photometer attached to a 50 cm telescope to monitor the position of SGR 0526−66 for 910 hr. Three optical bursts were detected, but no γ-ray events were detected in coincidence with these events. Furthermore, there was insufficient information on backgrounds to unambiguously identify the optical flashes with SGR 0526−66. The three events peaked around $m_V \sim 9$ for a few milliseconds. Assuming that SGR 0526−66 is at a distance of 50 kpc (see, e.g., Bergeat, Knapik, & Rutily 1988), and correcting for a reddening of $E(B-V) = 0.37$ mag (Vancuraet al. 1992), this corresponds to $L \sim 8 \times 10^{38}$ ergs s^{-1} at the peak. Unfortunately, the shortest ROTSE-1 exposures of 5 s reach a limit $m_{\rm ROTSE} \sim 13$ averaged over the exposure length. Therefore, the luminosity limit in equation (1) for SGR 1900+14 is a factor of $\sim$20 too large to detect flashes similar to those observed by Pedersen et al. (1984).

2.2.6. *Future ROTSE Observations of SGRs*

With the large extinction in the direction of the known SGRs, a campaign specifically designed to detect SGRs would utilize a rapid-response detector sensitive in the 1–10 μm region of the spectrum. However, ROTSE-I will continue to observe SGR triggers since doing so is a simple extension of ROTSE's main GRB response program. Furthermore, the ROTSE collaboration is developing several 45 cm aperture telescopes which should be $\sim$5 mag more sensitive than ROTSE-I and may be sensitive enough to detect optical emission from SGR 1900+14 at the level Pedersen et al. (1984) reported for SGR 0526−66 or the nebular emission discussed in § 2.2.4.

3. CONCLUSION

We have presented the first limits on optical emission immediately following SGR bursts for 10 events. Limits on optical transient counterparts are in the range $m_{\rm ROTSE} \approx$ 12.5–15.5 during the period 20 s to 1 hr after the bursts. For the eight events from SGR 1900+14, these limits correspond to extinction-corrected absolute magnitudes of $M \sim -8$. A more sensitive ROTSE telescope currently being developed may be sufficiently sensitive to detect optical emission from a flaring nebula surrounding SGR 1900+14 or emission similar to that possibly seen for SGR 0526−66.

We acknowledge useful discussions with Richard Epstein and Tom Vestrand and thank Brad Edwards for assistance measuring the Canon lens response. We thank Ersin Gögüs, Peter Woods, and the BATSE team for providing SGR peak flux and fluence values. ROTSE is supported by NASA under SR&T grant NAG 5-5101, the NSF under grants AST 97-03282 and AST 99-70818, the Research Corporation, the University of Michigan, and the Planetary Society. Work performed at LANL is supported by the DOE under contract W-7405-ENG-36. Work performed at LLNL is supported by the DOE under contract W-7405-ENG-48.

REFERENCES

Atteia, J.-L., et al. 1987, ApJ, 320, L105
Barthelmy, S. D., et al. 1995, Ap&SS, 231, 235
Bergeat, J., Knapik, A., & Rutily, B. 1998, A&A, 332, L53
Bertin, E., & Arnouts, S. 1996, A&AS, 117, 393
Cardelli, J. A., et al. 1989, ApJ, 345, 245
Cline, T. L., Mazets, E. P., & Golenetskii, S. V. 1998, IAU Circ. 7002
Cline, T. L., et al. 1982, ApJ, 255, L45
Duncan, R. C., & Thompson, C. 1992, ApJ, 392, L9
Fishman, G. J. et al. 1989, in Proc. GRO Science Workshop, Goddard Space Flight Center, ed. W. N. Johnson (Greenbelt: NASA/GSFC), 2–39
Frail, D. A., et al. 1999, Nature, 398, 127
Gorenstein, P. 1975, ApJ, 198, 95
Høg, E., et al. 1998, A&A, 335, L65
Hurley, K., et al. 1999a, ApJ, 510, L107
———. 1999b, ApJ, 510, L111
———. 1999c, Nature, 397, 41
———. 1999d, ApJ, 523, L37
———. 2000, ApJ, 528, L21
Kehoe, R., et al. 2000, in The STScI May Symposium, The Largest Explosions since the Big Bang: Supernovae and Gamma Ray Bursts, ed. M. Livio, N. Panagia, & K. Sahu (Baltimore: STScI), in press
Kouveliotou, C., et al. 1987, ApJ, 322, L21
———. 1998, Nature, 393, 235
Kouveliotou, C., et al. 1999, ApJ, 510, L115
Kulkarni, S. R., & Frail, D. A. 1993, Nature, 365, 33
Laros, J. G., et al. 1987, ApJ, 320, L111
Manchester, R. N., & Taylor, J. H. 1977, Pulsars (San Francisco: Freeman)
Mazets, E. P., & Golenskii, S. V. 1981, Ap&SS, 75, 47
Mazets, E. P., et al. 1979, Nature, 282, 587
———. 1999, Astron. Lett., 25, 635
Murakami, T., et al. 1994, Nature, 368, 127
Norris, J. P., et al. 1991, ApJ, 366, 240
Pedersen, H., et al. 1984, Nature, 312, 46
Rothschild, R., Kulkarni, S., & Lingenfelter, R. 1994, Nature, 368, 432
Sonobe, T., et al. 1994, ApJ, 436, L23
Tavani, M. 1994, ApJ, 431, L83
Taylor, J. H. & Cordes, J. M. 1993, ApJ, 411, 674
Thompson, C. & Duncan, R. C. 1995, MNRAS, 275, 255
Thomson-CSF Semiconductors Specifiques. 1995, CCD Products, Publ. DB CCD/0196 (1995 December)
Vancura, O., Blair, W. P., Long, K. S., & Raymond, J. C. 1992, ApJ, 394, 158
Vasisht, G., et al. 1994, ApJ, 431, L35
Vrba, F. J., et al. 1996, ApJ, 468, 225
Woods, P., et al. 1998, IAU Circ. 6948
Woods, P. M., et al. 1999, ApJ, 519, L139